Routine determination of plankton community composition and size structure: a comparison between FlowCAM and light microscopy

EVA ÁLVAREZ*, MARTA MOYANO[†], ÁNGEL LÓPEZ-URRUTIA, ENRIQUE NOGUEIRA AND RENATE SCHAREK
INSTITUTO ESPAÑOL DE OCEANOGRAFÍA, CENTRO OCEANOGRÁFICO DE GIJÓN, 33212 GIJÓN, SPAIN

[†]PRESENT ADDRESS: INSTITUTE FOR HYDROBIOLOGY AND FISHERIES SCIENCE, UNIVERSITY OF HAMBURG, OLBERSWEG, 24, 22767, HAMBURG, GERMANY.

*CORRESPONDING AUTHOR: eva.alvarez@gi.ieo.es

Samples from a monthly monitoring programme in the Cantabrian Sea were analysed with a FlowCAM-based automated technique. The estimates of abundance, biomass size spectra and taxonomic diversity of nano- and microplankton communities were compared with those obtained by traditional microscopical analysis of the same samples. The structure and abundance of a preserved plankton sample determined using FlowCAM showed minimal differences compared with traditional microscopical estimates. The effects of sample preservation and inaccuracies in the automatic classification are the main causes of discrepancies in the size structure determination between the two approaches. However, the synoptic understanding of the seasonal variation in the abundance, biomass and diversity obtained from the two methods is similar. Our results suggest that the natural variations in the community attributes explored are of greater magnitude than the error introduced by the methods and that the fully automatic method is adequate to explore these variations.

INTRODUCTION

The demanding task of gathering information on plankton composition and abundance has traditionally relied on taxonomists who identify and enumerate specimens under the microscope. The Utermöhl method is the most widely used protocol to enumerate nano- and microplankton (Utermöhl, 1958). To estimate cell biovolume, experts describe each taxonomic group by a geometrical shape (Hillebrand *et al.*, 1999), and estimate a suitable number of linear dimensions, either by direct measurement or by using known aspect ratios (Olenina *et al.*, 2006). This traditional method is highly time-consuming and thus imposes limitations on the number of samples that can be processed. In addition, the use of fixatives to preserve samples introduces biases in the biovolume estimates due to cell shrinkage (Montagnes *et al.*, 1994). This traditional technique is considered to be the most accurate for the identification and enumeration of nano- and microplankton and is the benchmark methodology. Nevertheless, several human factors such as fatigue and inexperience of the operator can affect the quality of the analysis (Culverhouse *et al.*, 2003).

Over the past two decades, combinations of automated sampling devices, image analysis technologies and machine learning algorithms have been developed to count and size plankton organisms more rapidly (Benfield *et al.*, 2007). However, all methods for plankton enumeration have uncertainties when estimating the actual composition and abundance of the community, and the proper interpretation of the results requires assessment of the confidence limits of each method. The reliability of the data provided by new automated methods based on image analysis is still under assessment. There is a need to demonstrate their benefits and disadvantages through comparison against the standard, traditional methods (Jakobsen and Carstensen, 2011).

The Flow Cytometer And Microscope (FlowCAM) is an automated technique for particle enumeration that combines flow cytometry and microscopy (Sieracki *et al.*, 1998). It adds to the growing collection of methods for plankton enumeration based on image analysis. The characteristic step of all these systems is representation of the organisms present in a water sample by a set of images, a process called digitalization. In the FlowCAM, digitalization is based on the capture of images from a water sample flowing through a rectangular glass chamber, the flow cell. A microscope lens coupled to the digital camera magnifies the particles up to 200 times and a calibration factor (microns per pixel) provides their actual size. Depending on the instrument setup and microscope objective used, the FlowCAM can detect cells or particles that range from 3 to 3000 μm in size. One advantage of FlowCAM is that samples can be digitized *in vivo* eliminating the need for preservation (Zarauz and Irigoien, 2008). Image analysis of FlowCAM digitized images provides precise estimates of the abundance and size of particles (Sieracki *et al.*, 1998; See *et al.*, 2005; Buskey and Hyatt, 2006; Ide *et al.*, 2008; Álvarez *et al.*, 2011). Automatic classification techniques based on pattern recognition provide accuracies reliable enough for most ecological studies (Blaschko *et al.*, 2005; Zarauz *et al.*, 2009; Álvarez *et al.*, 2012). However, traditional microscopy can easily identify cells to the species level, whereas automated methods that utilize automatic classification of images (obtained from FlowCAM or other automatic sampling devices) usually attain a taxonomic level of genus or above. The tendency to misestimate cell biovolume due to the two-dimensionality of the images can be overcome with the currently applied analysis algorithms that take into account the three-dimensional shape of the particles in estimating their biovolume (Álvarez *et al.*, 2012; Moberg and Sosik, 2012). Hence, FlowCAM sampling coupled with an automatic classification of the images generated aims to obtain information comparable with that provided by microscopy but with minimum human intervention, considerably reducing the sample processing time and the dependence on the operator.

FlowCAM can be considered complimentary to microscopy. It provides an analysis with low taxonomic resolution at a high rate, while traditional microscopy can achieve higher taxonomic resolution for a lesser number of samples. Nevertheless, the estimates of abundance, size structure and taxonomic composition obtained by both methods should be comparable. The aim of this work is to assess the similarity in the characterization of nano- and microplankton communities obtained with FlowCAM and with traditional microscopy. Sample acquisition for the comparison was simultaneous, but sample treatment and counting strategy followed the specific protocol for each method. The intention was to compare not only the counting and sizing ability of the methods, but their full capability to characterize the attributes of the plankton community.

METHOD

Monthly sampling was carried out in the central Cantabrian Sea in the framework of the time series monitoring program RADIALES (Oceanographic Time Series Program; http://www.seriestemporales-ieo.com).

Seawater samples were taken with a rosette sampler system at 2, 30 and 75 m from November 2008 to March 2010 at a coastal station (46.42°N, 1.85°W, bottom-depth = 100 m). Subsamples (1 L) to be analysed fresh with FlowCAM were pre-filtered at sea with a 200 μm mesh, kept fresh, stored in the dark and analysed in the laboratory within 3 h after collection. Subsamples (100 mL) for analysis of preserved samples with both microscopy and FlowCAM were poured into brown glass bottles with acid Lugol's solution and kept in the dark until analysis.

FlowCAM counts

Fresh samples were analysed with FlowCAM using two working modes. In autoimage mode, FlowCAM takes photographs at a fixed rate and the net sample volume imaged depends on the number of photographs taken. In fluorescence-triggered mode, digital images are taken of only those particles that emit red fluorescence, and the net sample volume imaged is roughly a third of the volume poured into the instrument. In both working modes, FlowCAM images only a subset of the particles in the sample and calculates their concentration taking into account the net sampled volume. An un-concentrated subsample was filtered with a 53 μm mesh and used for analysis at ×200 magnification (×20 objective and 50 μm flow cell), both in autoimage (20 000 photos, 30 min sample processing time) and in fluorescence-triggered mode (1 mL, 30 min sample processing time). A concentrated subsample (1 L down to around 20 mL) was filtered with a 100 μm mesh and used for analysis at ×100 magnification (×10 objective and 100 μm flow cell), both in autoimage (20 000 photos, 30 min sample processing time) and in fluorescence-triggered mode (10 mL, 30 min sample processing time). To minimize the damage to living cells, samples were concentrated by reverse filtration (Dodson and Thomas, 1978) through a 15 μm mesh. The preserved samples were not concentrated because of the small volume of the sample. They were analysed in two working modes: autoimage and side-scatter-triggered. In the latter, FlowCAM digitizes all particles scattering light and the net sample volume imaged is roughly a third of the volume poured into the instrument. Preserved samples were filtered with a 53 μm mesh and analysed at ×200 magnification in autoimage mode (40 000 photos, 1 h sample processing time) and filtered with a 100 μm mesh and analyzed with ×100 magnification in side-scatter-triggered mode (15 mL, 3 h sample processing time). Hence, three subsamples described each sample: one analysed in fluorescence-triggered mode to account for the autotrophic nano- and microplankton community, one analysed in autoimage mode to account for the whole nano- and microplankton community in fresh samples and one analysed in both autoimage and side-scatter-triggered mode to account for the whole nano- and microplankton community in preserved samples.

Classification of FlowCAM images

For preserved samples, the images were sorted as living versus non-living particles by visual inspection. Biovolume was calculated from the equivalent spherical diameter of the particle (called ABD diameter in the FlowCAM software), corrected for shrinkage (Montagnes et al., 1994) and converted to carbon content (Menden-Deuer et al., 2000). For fresh samples, in order to obtain taxonomic information from the FlowCAM images, we applied the automatic classification technique described by Álvarez et al. (Álvarez et al., 2012). Briefly, the technique applies an image analysis algorithm to describe numerically each image recorded by the FlowCAM. The Support Vector Machine (SVM) algorithm then separates the particles into 34 groups. These 34 groups are merged from a taxonomic point of view into seven "functional classes" (diatoms, silicoflagellates, dinoflagellates, ciliates, crustaceans, other living particles and detritus) and from a morphological perspective as four "shape classes" (spheres, ellipsoids, cylinders and discs). Simplification of taxonomic categories permits comparison with other methods whose taxonomic resolution is not the same as that attained by the automatic classification. Morphological description of particles, although only as simple geometrical shapes, gives a better estimation of cell biovolume and allows comparison with methods not based on two-dimensional images. Hence, the automated classification of the samples produced both a functional class and a simple shape assignment for each image. Particle biovolume was calculated as a revolution volume appropriate to the assigned simple shape and the dimensions (length and width) measured by the image analysis. Biovolume was converted to carbon according to the functional class predicted. Different conversion factors were applied for cells smaller than 3000 μm^3, cells larger than 3000 μm^3 except diatoms and diatoms larger than 3000 μm^3 (Menden-Deuer et al., 2000).

Microscopy counts

For microscopical analyses, the samples preserved in Lugol's solution were enumerated following the Utermöhl technique (Utermöhl, 1958; Edler and Elbrächter, 2010). Between 25 and 50 mL of the sample were dispensed into settling chambers and cells were allowed to settle for at least 15 and up to 30 h. Cells were

counted with ×100, ×200 and ×400 magnifications using a NIKON inverted microscope in evenly spaced stripes. Whenever possible, organisms were classified at the species or genus level. A total of 144 taxonomic groups were identified in the 17 samples analysed. Some of these taxa were separated into several size classes (e.g., *Chaetoceros* subgenus *Phaeoceros* $10-20\ \mu m$ and $20-40\ \mu m$) given their wide size ranges (Olenina *et al.*, 2006).
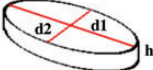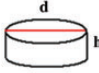
Biovolume estimation on microscopy counts

The initial database for microscopical counts consists of a series of taxonomic groups and their estimated abundances in each sample. Starting from the taxonomic information, we made several inferences to obtain information about the biovolume and the trophic status of each taxonomic group. Table I shows an example of this treatment for a given taxon (*Chaetoceros compressus*). Each taxon was assigned to a functional class (diatoms, silicoflagellates, dinoflagellates, ciliates or other living particles) to match the taxonomic resolution of the FlowCAM (Supplementary data, Correspondances). In addition, each taxon was assigned to a trophic status (heterotrophic or autotrophic/mixotrophic) in order to make possible comparison with the results provided by the different FlowCAM working modes. The shape of each taxonomic group was defined according to composite geometric bodies extracted from the literature (Hillebrand *et al.*, 1999; Sun and Liu, 2003; Olenina *et al.*, 2006), obtaining a total of 24 composite shapes for the taxonomic groups present in the samples analysed. Those 24 composite shapes were simplified to three: sphere, ellipsoid and cylinder (Supplementary data, Correspondances). The linear measurements needed to describe a composite shape ranged from only one (e.g. sphere) to seven (e.g. flattened ellipsoid + cylinder + two

cones). For each taxonomic group, the range of these composite cell dimensions was taken from the literature (Cupp, 1977; Dodge, 1982; Tomas, 1997; Bérard-Therriault *et al.*, 1999; Olenina *et al.*, 2006). Since simple shapes are only defined by two linear measurements (length and width), composite cell dimensions were reduced to simple cell dimensions considering only the main body of the cell and its most likely orientation on a flat surface. Minimum and maximum cell biovolume for each taxonomic group was calculated as a revolution volume considering the simple shape and the range of cell dimensions. Cell biovolumes were converted to carbon as previously described (Menden-Deuer *et al.*, 2000).

Cell biovolume inferred from a subset of cells

An important difference between traditional and automated methods for plankton enumeration is the fact that with the latter it is possible to count and measure all cells imaged during the analysis of a sample. Traditional microscopic methods only allow measurement of a limited number of cells or use previously published cell dimensions. In order to analyse the effect of measuring only a subset of cells during microscopical analyses, we used two approximations to assign biovolume to each of the cells counted in the taxonomic group. First, the biovolume of every cell counted was assumed to be equal to the average biovolume of the taxon ("average biovolume"), which is the most widely used method for analysis of the size structure of nano- and microplankton using microscopy (e.g. Cermeño and Figueiras, 2008; Huete-Ortega *et al.*, 2010). However, cells within a population do not have equal sizes, rather their biovolumes distribute within the range defined by the maximum and

Table I: Example of the treatment given to each taxonomic group found in the microscopy counts to obtain information about the biovolume of each cell

Taxonomical group	Functional class	Tropic status	Composite shape			Simple shape		
Chaetoceros compressus	Diatoms	Autotrophic	Oval cylinder			Cylinder		
			Composite cell dimensions (µm)	min	max	Simple cell dimensions (µm)	min	max
			Height (h)	5	14	Height (h)	5	14
			Diameter (d1)	5	10	Diameter (d)	5	10
			Diameter (d2)	4.25	8.5			
Biovolumerange of the group:						Min and max simple biovolumes		

Two biovolume data sets were considered: average and distributed biovolume. Composite shape and cell dimensions from Olenina *et al.* (2006). See online supplementary data for a colour version of this table.

the minimum of the species. Consequently, the second approximation assigns a biovolume to each cell within the biovolume range of the group ("distributed biovolume"). In the case of species counted only in one size category, we considered the cell biovolumes to be normally distributed and assigned a random-Normal value from a distribution with the appropriate mean size and a standard deviation equal to 0.21 times the range (maximum–minimum). In the case of groups combining several species (i.e. Ciliates) or species divided in several size classes (i.e. the taxonomist counted cells of taxon in two size categories; for example, *Chaetoceros* subgenus *Phaeoceros* 10–20 µm and *C.* sg *Phaeoceros* 20–40 µm), we considered uniform distributions of biovolumes.

Size spectra

In order to establish a basis for further comparisons, the characteristics of the community were estimated separately for distinct biovolume classes. In order to obtain the abundance size spectrum (ASS) and the biomass size spectrum (BSS), cell abundance (cells L^{-1}) and biomass (µg C L^{-1}) were distributed in biovolume classes established on an octave scale, from 2^4 to 2^{18} µm^3 in biovolume, which corresponds to a size range from 3 to 100 µm of equivalent spherical diameter. The ASS and the BSS conform to a power law:

$$N_s = a \times S^b \qquad (1)$$

where s is the lower limit of the biovolume class, s is also the width of the class interval, N is the abundance in the biovolume class and a and b are the parameters of the power law. The ASS and the BSS were normalized by dividing each class by its width in biovolume units (Δs), obtaining the normalized abundance size spectrum (NASS) and the normalized biomass size spectrum (NBSS), both of which follow a linear relationship when plotted in a log–log scale:

$$\log\left(\frac{N_S}{\Delta S}\right) = \log(a) + b \times \log(S) \qquad (2)$$

The slope (b) and the intercept ($\log(a)$) of the NASS for each sample were estimated by fitting a linear regression model to the points of each normalized spectrum. To avoid biases in the calculation of the spectra due to curvature at the extremes of the size range, we rejected those biovolume classes with less than 5 cell counts or located to the left of the modal class (García *et al.*, 1994).

Diversity

Species diversity may be defined as a measure of species composition, in terms of both the number of species and their relative abundances (Legendre and Legendre, 1998). The taxonomic richness (S) simply takes into account the number of taxonomic groups present in the community, whereas higher order indices, such as Shannon's index (H), consider also the relative abundance of each group:

$$H = -\sum_{i=1}^{q} p_i \times \log(p_i) \qquad (3)$$

where q is the number of taxonomic groups and P the abundance of each group relative to the total abundance. Indices S and H were estimated from both FlowCAM and microscopical counts. For microscopy data, we considered the 144 taxonomic groups identified and their abundances, whereas for FlowCAM data, we used the 34 groups and their abundances provided by the automatic classification. The calculation of diversity indices only considered individuals in reliably sampled biovolume classes. A biovolume class was considered reliably sampled when the abundance obtained with FlowCAM did not exceed double or fall below half of the abundance obtained with light microscopy.

RESULTS

Size spectra estimation from microscopy counts

As previous studies have shown, there are no significant differences between composite shapes and simple shapes for estimating the biovolume of cells in order to characterize size spectra (Menden-Deuer *et al.*, 2000), with the advantage that the latter method requires measurement of only two cell dimensions. The most widely used biovolume method for microscopy is to estimate an average for a subset of cells and assign that average biovolume to all cells of a given taxon. That is not realistic. When we measured every cell counted during analysis of a sample using the FlowCAM analysis, distributions of cell biovolumes emerged (Fig. 1). The biovolume distributions estimated from FlowCAM images for four exemplary species of microplankton span at least two biovolume classes of the size spectra (delimited by the vertical lines in Fig. 1). These biovolume distributions were approximately Normal. Hence, to infer the Normal distribution for the species analysed by microscopy for which only the biovolume range was available, we calculated the ratio between the standard deviation of the biovolume distribution and the biovolume range based on these four exemplary species. This ratio was very similar for the four species (0.2125 ± 0.0374). Hence, the Normal distribution for each species was calculated using the average of the
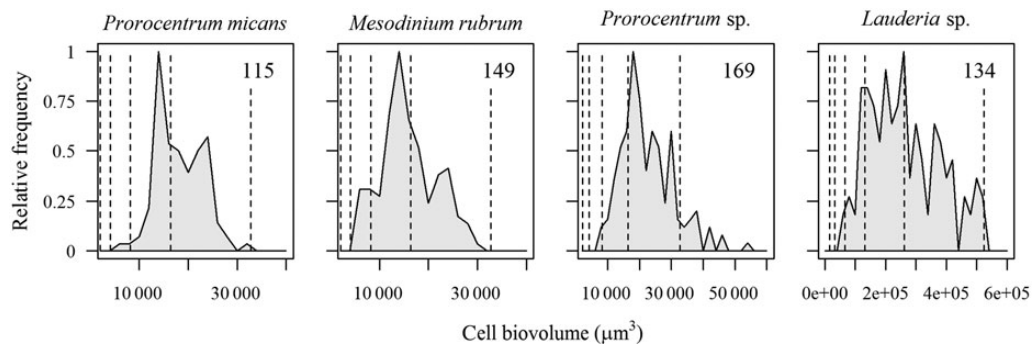
Fig. 1. Biovolume frequency for cells of four selected species present in natural samples analysed with FlowCAM: *Prorocentrum micans*, *Prorocentrum* sp. (dinoflagellates), *Mesodinium rubrum* (ciliate) and *Lauderia* sp. (chain-forming diatom). Vertical lines show the limits of the biovolume classes of the size spectra to indicate how a single species can spread through several biovolume classes. The number in the upper right corner of each panel indicates the total number of cells.
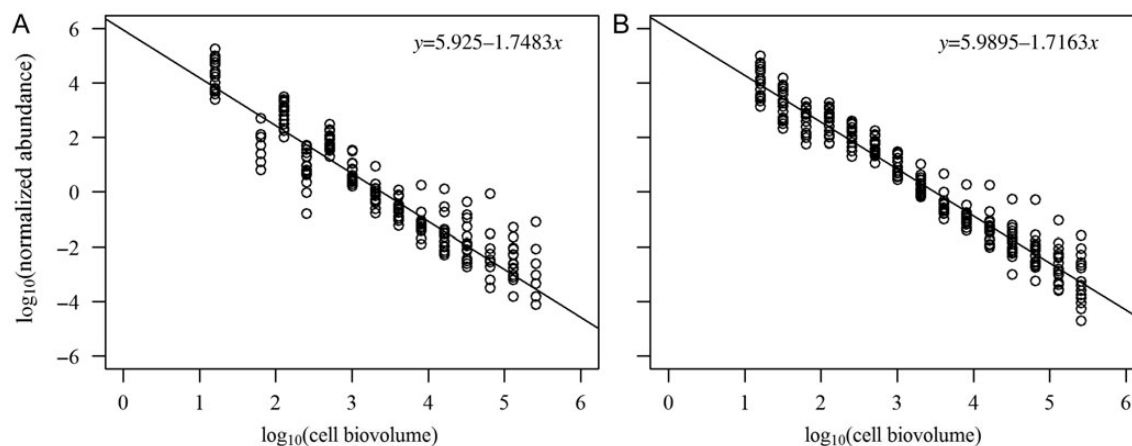

Fig. 2. Normalized abundance size spectra of analysed samples (NASS) from microscopy counts for (**A**) the "average biovolume" data set and (**B**) the "distributed biovolume" data set.

biovolume range limits and 0.2125 times that range as the standard deviation. The NASS constructed using this new abundance distribution for each taxon in its biovolume range (Fig. 2B) do not show the peak-valley pattern of the average biovolume spectra (Fig. 2A), in which several classes had abundance/biomass lower than expected, whereas other bins had higher abundances/biomass.

To determine which parameters of the size spectra (slope and/or intercept) were affected, we compared both methods of biovolume assignment (average and distributed) in the microscopy data sets (Fig. 3). The slopes of the average and distributed NASS were not statistically different ($P = 0.0830$, $n = 17$), whereas the intercepts were significantly different ($P < 0.0001$, $n = 17$). To determine which parts of the size spectra were most affected, we compared the means of the abundance and

biomass in each biovolume class for the average and distributed microscopy data sets using a Student's t-test (Fig. 4). Artefacts in the average biovolume data set were more conspicuous in the smallest biovolume classes. When applying the distribution of biovolume to the counts of each taxonomic group, the variability between contiguous biovolume class decreases. When comparing the mean abundance and biomass for each biovolume class, as determined by the average and distributed data sets, significant differences appeared in the biovolume classes below 10 μm ESD ($P < 0.05$, $n = 17$). The differences between the two data sets for the remaining biovolume classes were not significant. Differences in the larger size classes, however, cannot be ruled out, as the power of the statistical test is reduced due to the smaller numbers of cells in the larger biovolume classes.
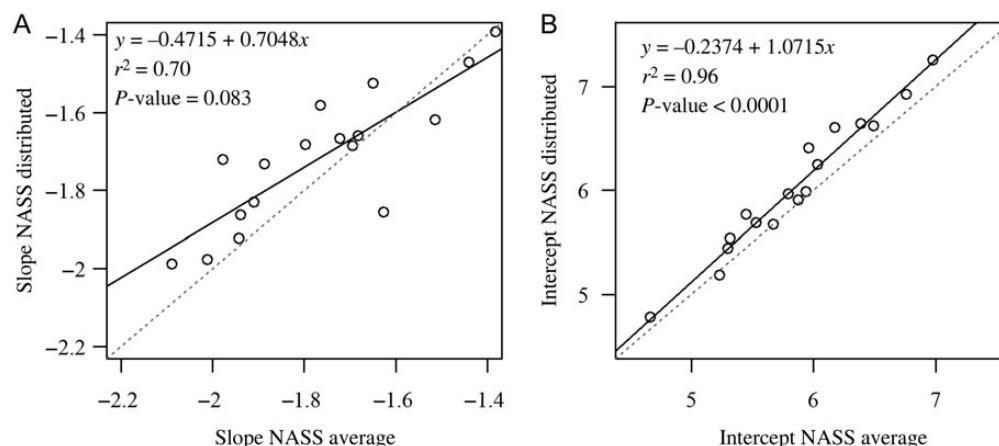
Fig. 3. Comparison of the parameters of the NASS, (**A**) slope and (**B**) intercept, constructed using the "average biovolume" data set (*x*-axis) versus the "distributed biovolume" data set (*y*-axis) from microscopy counts. For each parameter, the slope, the *r*-squared of the relationship and the *P*-value of the *t*-test that examines whether the relationship is 1:1 are displayed. The grey dotted line shows the 1:1 relationship.
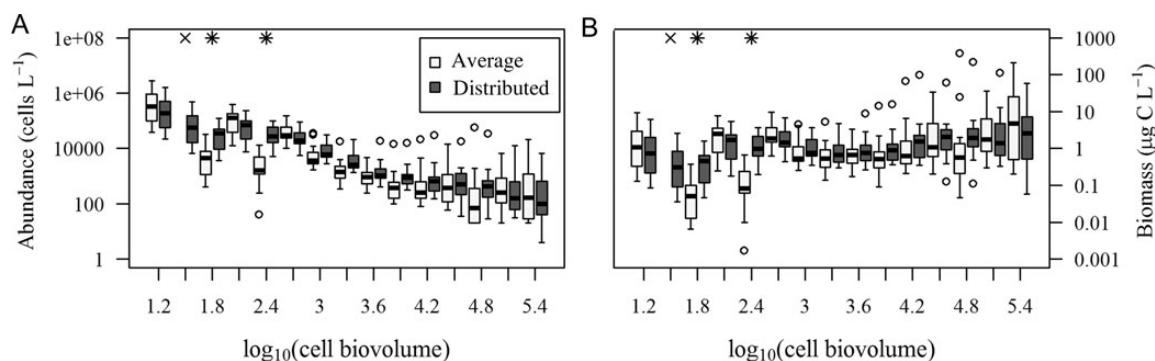

Fig. 4. Box and whisker plot for comparison of the mean (dark bar), standard deviation (box) and range (whisker) of (**A**) the abundance (cells L^{-1}) and (**B**) biomass (μg C L^{-1}) in each biovolume class calculated with the "average biovolume" and the "distributed biovolume" data sets from microscopy counts. Biovolume classes are indicated for which the means were different by Student's *t*-test (* above) and where the comparison was not possible because the bin was absent from one of the data sets (× above).

Comparison between FlowCAM and light microscopy

Analysis of the intra-method variability has been reported previously for FlowCAM, as well as for light microscopy. Previous studies evaluated the variability of FlowCAM measurements by triplicate counting of single-species cultures, obtaining coefficients of variation (cv) within replicates ranging only from 2 to 11% for the fluorescence-triggered mode (Sieracki *et al.*, 1998) and from 6.6 to 53.0% when considering the three FlowCAM working modes (12.4% in autoimage, 6.6% in fluorescence triggered and 53.0% in side-scatter triggered mode) (Álvarez *et al.*, 2011). Microscopical counts of subsamples analysed by the same taxonomist yield cv's ranging from 4 to 19%, increasing to 13–42% when the samples are counted by different experts (Willén, 1976; Vuorio *et al.*, 2007). To include the effect of this

intra-method variability in the comparison between FlowCAM and microscopy, we established a margin of error of 100% as an acceptable threshold, meaning that the difference in estimated cell concentrations between the methods is lower than a factor of two. The comparisons between FlowCAM and microscopy counts for each sample included estimates of abundance, biomass and community attributes such as size structure and diversity. The results obtained with FlowCAM for preserved and fresh samples in autoimage mode were compared with the distributed biovolume data set obtained with microscopy. The results obtained with FlowCAM in fluorescence-triggered mode were compared with the distributed biovolume data set obtained with microscopy only for autotrophic cells.

Figure 5 shows the abundance (cells L^{-1}) and biomass (μg C L^{-1}) per biovolume class estimated with microscopy
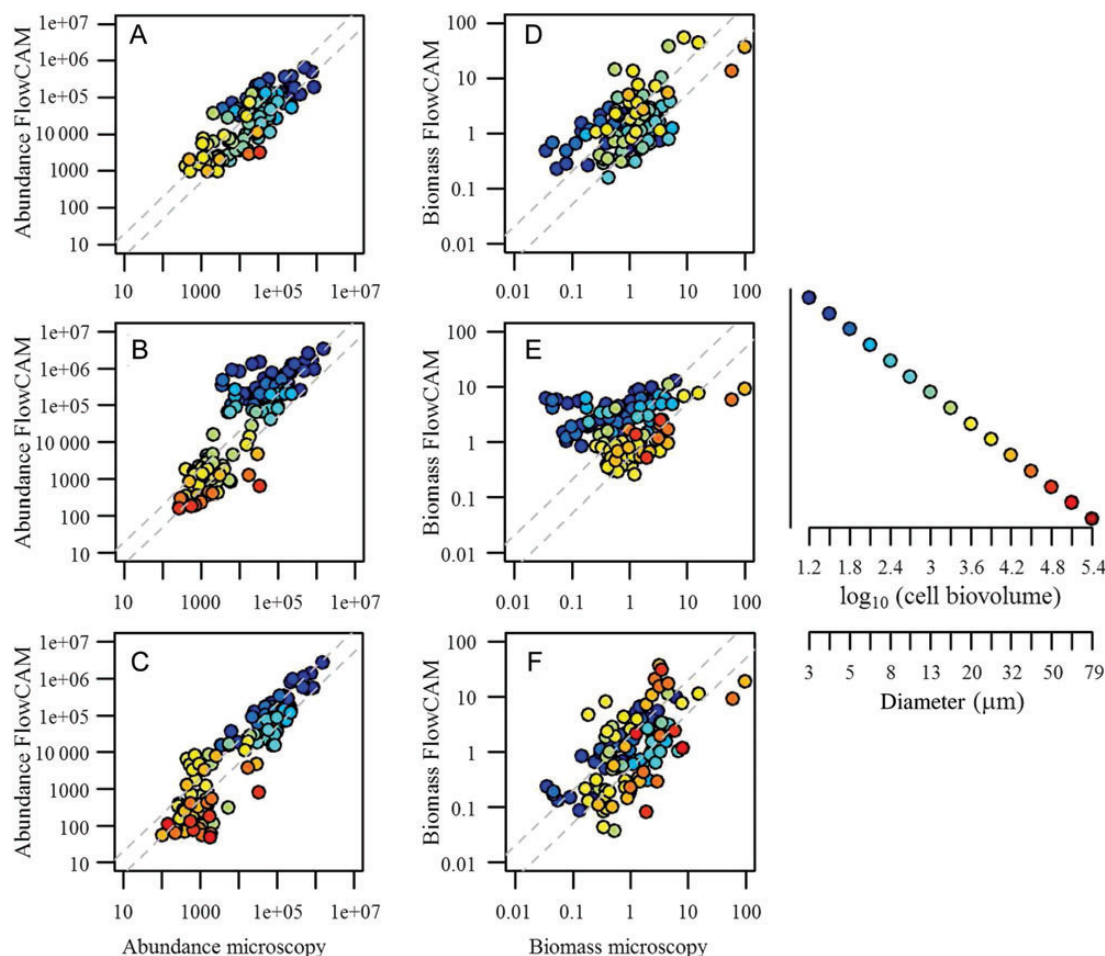
Fig. 5. Comparison of abundance (cells L^{-1}) (left panels) and biomass (μg C L^{-1}) (right panels) obtained with light microscopy (*x*-axis) versus the abundance or biomass obtained with FlowCAM (*y*-axis) in each biovolume class of the size spectra for (**A** and **D**) preserved samples and fresh samples analysed in (**B** and **E**) autoimage and (**C** and **F**) fluorescence-triggered mode. The colour of the point indicates to which biovolume class the abundance/biomass belongs, and the schematic size spectrum to the right shows the distribution of colours. The dashed lines represent the 100% scatter lines. See online supplementary data for a colour version of this figure.

against those estimated with FlowCAM. Differences arose in preserved samples as well as in fresh samples analysed in autoimage and fluorescence-triggered modes. Regarding abundance, the percentages of biovolume classes falling within a scatter area of 100% around the 1:1 relationship, were: 66.67% for preserved samples (Fig. 5A), 52.31% for fresh samples considering the total community (Fig. 5B) and 73.28% for fresh samples considering only autotrophic cells (Fig. 5C). In terms of biomass, the percentages of biovolume classes that meet the counting precision criteria of 100% were: 61.17% for preserved samples (Fig. 5D), 48.80% for the total community (Fig. 5E) and 68.14% when considering only autotrophic cells (Fig. 5F). For each FlowCAM working mode, the points deviating from the 1:1 relationship can be grouped by biovolume class. Whereas in the preserved samples, the error is homogeneously distributed, in the autoimage

samples the FlowCAM overestimated the smaller biovolume classes. On the other hand, FlowCAM generally underestimated larger biovolume classes in fresh samples.

Within functional classes (Fig. 6), there were differences in the abundance (cells L^{-1}) and biomass (μg C L^{-1}) per biovolume class estimated with microscopy and FlowCAM on fresh samples analysed with autoimage (Fig. 6A for ASS and Fig. 6C for BSS) and with fluorescence-triggered modes (Fig. 6B for ASS and Fig. 6D for BSS). Table II shows the percentages of biovolume classes that fall in the 100% scatter area around the 1:1 relationship. The percentage is relatively high for diatoms (from 64.29 to 84.31%) and dinoflagellates (from 86.67 to 100.00%), and lower for ciliates (from 33.33 to 62.50%), silicoflagellates (50.00 to 60.00%) and other living particles smaller than 20 μm (from 15.49 to 66.13%). Particularly low is the percentage of other living particles larger that
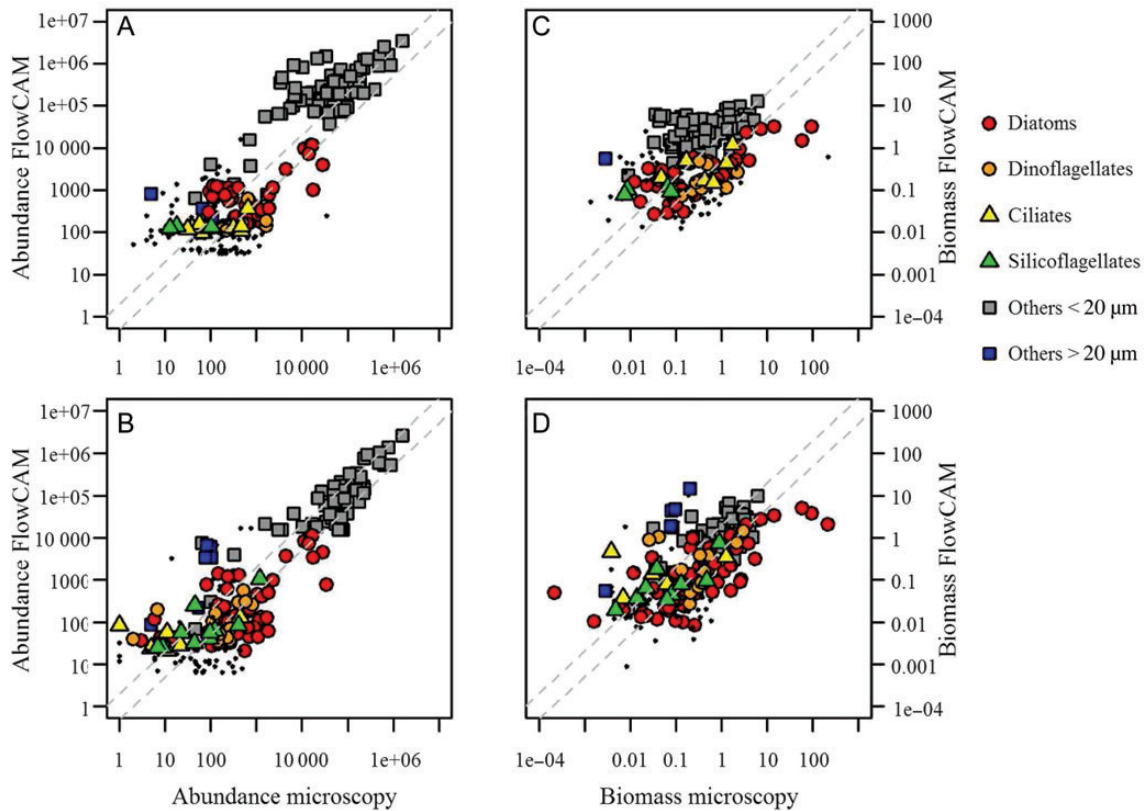
Fig. 6. Comparison of abundance (cells L^{-1}) (left panels) and biomass (μg C L^{-1}) (right panels) obtained with light microscopy (*x*-axis) versus the abundance/biomass obtained with FlowCAM (*y*-axis) in each functional class for fresh samples analysed in (**A** and **C**) autoimage and (**B** and **D**) fluorescence-triggered modes. The colour and shape of the point indicates to which functional class the abundance/biomass belongs. The dashed lines represent the 100% scatter lines. See online supplementary data for a colour version of this figure.

Table II: Percentage of biovolume classes of the size spectra for each functional class whose difference in estimated cell concentrations between FlowCAM and microscopy was less than a factor of two, which means a margin of error of 100%

Variable	Community	Others <20 μm	Others >20 μm	Diatoms	Dinoflagellates	Ciliates	Silicoflagellates
Abundance	Total	21.33	16.67	64.29	100.00	62.50	50.00
	Autotrophic	66.13	14.29	80.77	86.67	50.00	60.00
Biomass	Total	15.49	0.00	71.05	100.00	62.50	50.00
	Autotrophic	61.67	14.29	84.31	86.67	33.33	60.00

"Total nano- and microplankton community" compares the results obtained with FlowCAM in autoimage mode with all cells counted in microscopy, whereas the "autotrophic community" compares the results obtained with FlowCAM in fluorescence-triggered mode to only the autotrophic cells counted with microscopy.

20 μm (from 0.00 to 16.67%). The catch-all nature of the group "others > 20 μm" in the FlowCAM methodology explains its poor comparison. This group is designated as living particles that are not classified within a functional class due to the poor FlowCAM image quality. It is a group that is usually absent in traditional microscopy analyses, since cells greater than 20 μm are usually always classified. In the "others < 20 μm" group, there are large differences in the accuracy of fluorescence-triggered

(63.90% on average) and autoimage modes (18.41%), due, as seen previously, to the overestimation of small cells by the FlowCAM in autoimage mode.

Regarding community attributes, we explored the size structure and the diversity of the samples obtained with both methodologies. Figure 7 compares the parameters of the NASS from microscopy counts with the parameters of the NASS from FlowCAM. The adjustments to the 1:1 relationship of the slopes of the NASS from
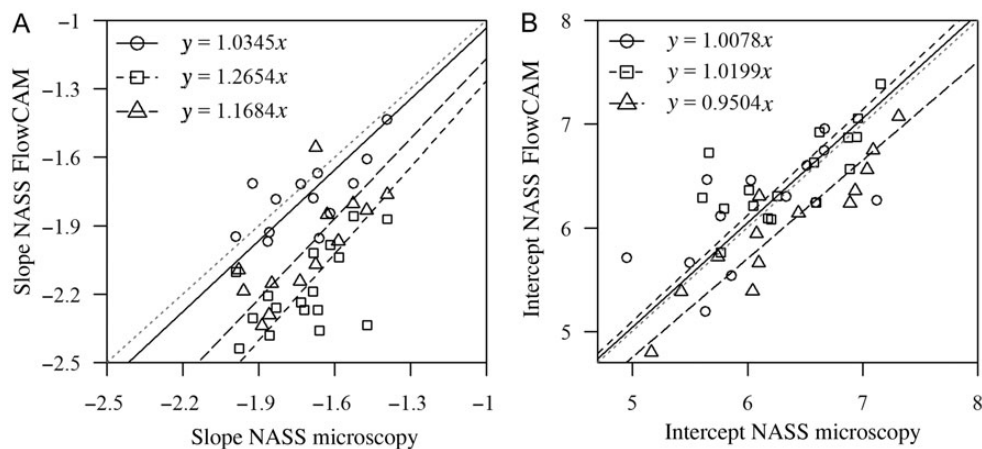
Fig. 7. Comparison of the parameters of the NASS, (**A**) slope and (**B**) intercept, obtained with light microscopy versus the parameters obtained with FlowCAM on preserved samples (circles and solid line) and FlowCAM on fresh samples analysed in autoimage (squares and short-dashed line) and in fluorescence-trigger mode (triangles and long-dashed line). The grey dotted line shows the 1:1 relationship.
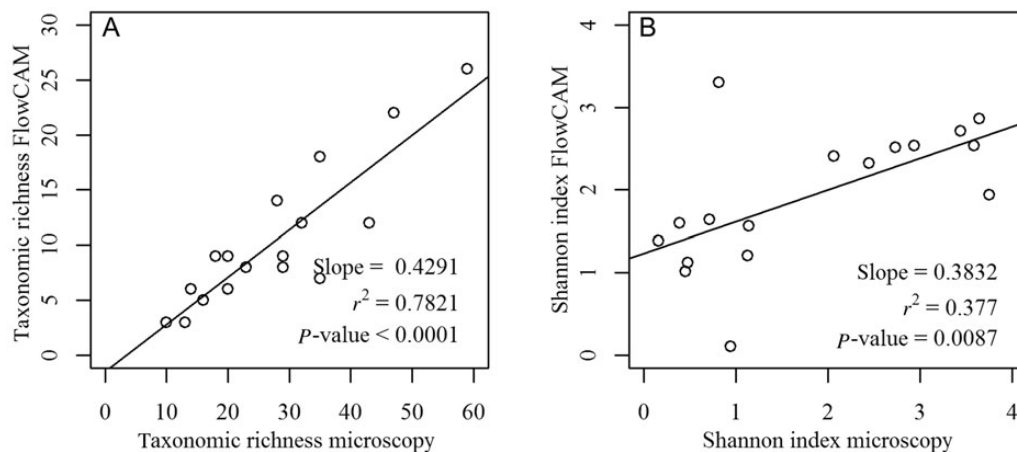

Fig. 8. Comparison of the diversity, (**A**) taxonomic richness and (**B**) Shannon index, for each sample obtained with light microscopy against the diversity obtained with the automatic classification of FlowCAM images. For each index, the slope, the *r*-squared of the relationship and the *P*-value of the *t*-test that examines whether the correlation is significant are displayed.

microscopy against FlowCAM were tested with a Student's *t*-test. When the slopes were not significantly different, the intercepts were calculated assuming a constant slope, and the 1:1 relationship between the intercepts of FlowCAM and microscopy were tested with a *t*-test. The slope relationship for preserved samples was not different from the 1:1 line (slope: $P = 0.1434$, intercept $P = 0.7265$, $n = 13$). The relationships were different from the 1:1 relationship for fresh samples analysed with FlowCAM in autoimage and preserved samples with microscopy (slope: $P < 0.0001$, $n = 17$), and for the fluorescence-triggered mode (slope: $P < 0.0001$, $n = 13$).

Figure 8 shows the comparison of diversity indices obtained for each sample with both methodologies. Obviously, the categories the classification tool was trained to discriminate limit the maximum number of groups that can appear in FlowCAM samples. An image of an organism whose taxon was not included in the training set of images is assigned to one or another of the pre-defined categories. On the other hand, the taxonomic resolution of traditional microscopy is limited by the expertise of the taxonomist who can identify a new taxon even when it has not been observed in previous samples. Therefore, the relationship between diversity indices is not expected to fit a 1:1 relationship, and consequently the correlation between the estimates provided by FlowCAM and microscopy was evaluated with a Student's *t*-test and by reporting the value of *r*-squared for each diversity index. For taxonomic richness, the correlation was significant ($P < 0.0001$, $n = 17$) and the r^2 was 0.78. For the Shannon index, although the
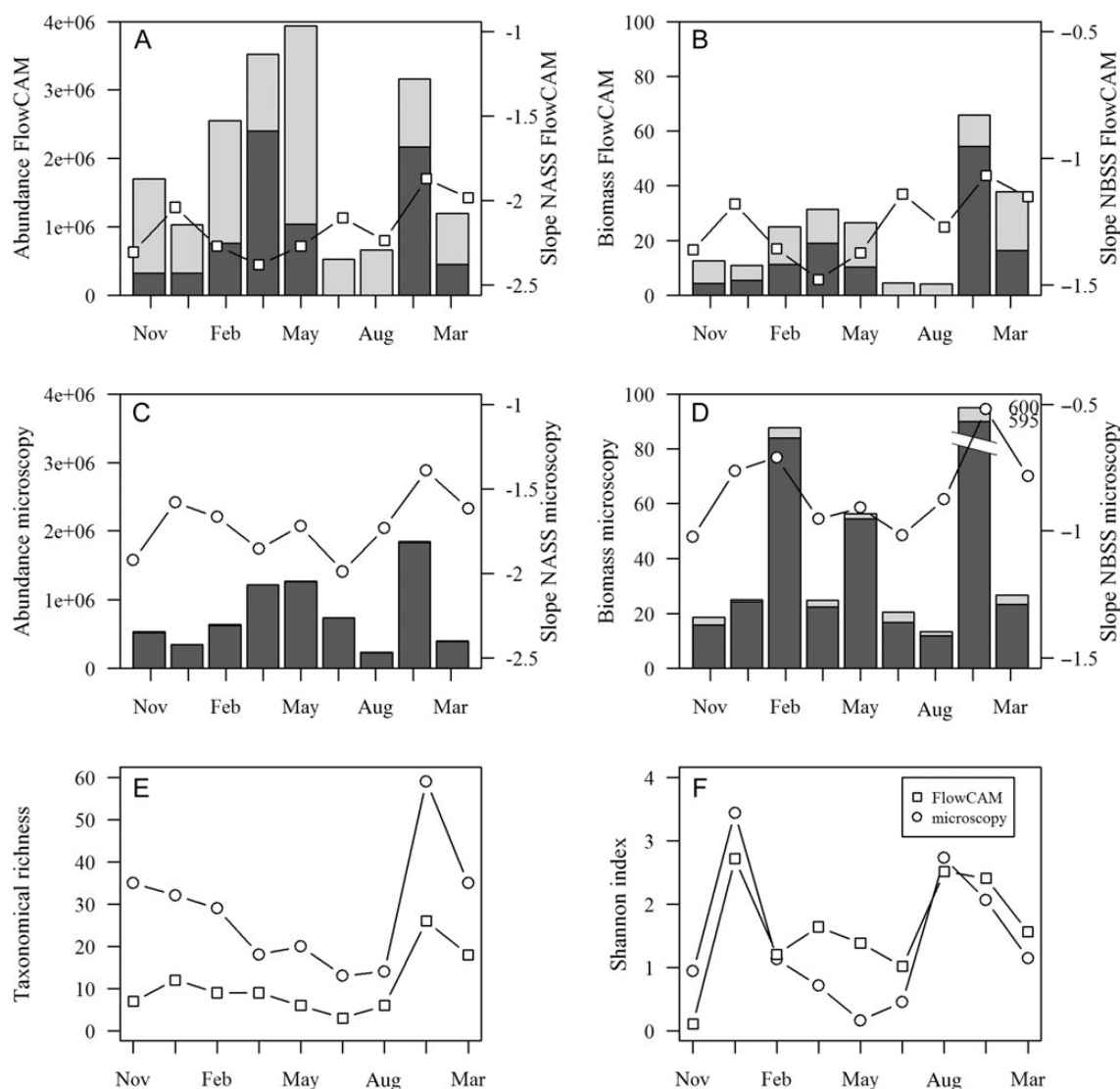
Fig. 9. Variation in the community attributes explored in the work during the sampling period at the surface of a coastal station (46.42°N, 1.85°W, bottom-depth = 100 m). Abundance of cells (autotrophic in dark grey bars and heterotrophic in light grey bars, cells L^{-1}) and slope of the NASS (points) with (**A**) FlowCAM and (**C**) light microscopy. Biomass (μg C L^{-1}) and slope of the NBSS with (**B**) FlowCAM and (**D**) light microscopy. Diversity indices: (**E**) taxonomic richness and (**F**) Shannon index.

correlation was also significant ($P = 0.0087$, $n = 17$), the r^2 was only 0.38.

Finally, the temporal variation of community attributes during the study period illustrates the output obtained by both methodologies (Fig. 9). The abundance (cells L^{-1}, Fig. 9A) and biomass (μg C L^{-1}, Fig. 9B) of nano- and microplankton estimated with FlowCAM followed the same pattern as the abundance (Fig. 9C) and biomass (Fig. 9D) estimated with microscopy. Thanks to the use of two different working modes, fluorescence triggered and autoimage modes, respectively, FlowCAM was capable of discriminating the autotrophic (dark grey bars) from the heterotrophic community (light grey bars) without

additional sample treatment. For the whole nano- and microplankton community and for the autotrophic community, the timing of maxima and minima of abundance and biomass matched. The same happened with the parameters of the size spectra as well as with the diversity indices explored (Fig. 9E and F). Although the trends were similar with both methodologies, the absolute values differed.

DISCUSSION

The scientific community has focused much effort on comparisons between automated and traditional techniques for plankton enumeration, given the growing interest

in the automated techniques. We have compared traditional light microscopy and the automatic, FlowCAM-based technique for routine analyses of nano- and microplankton samples. The wide sample variability covered, in both cell abundance and taxonomic composition, ensures the reliability of the comparison. This was attained by considering samples collected during a time series monitoring programme, which covered the whole seasonal cycle at different depths within the photic layer of the coastal Cantabrian Sea. Our results broaden knowledge about the reliability of automated methods, clarify which tasks the FlowCAM can tackle and which it currently cannot.

Performance of FlowCAM on routine sample analyses

Microscopy-based biovolume estimations have been the main source of information for size structure studies of nano- and microplankton. In most routine sample analyses, taxonomists measure only a subset of cells and assign a unique average biovolume to each taxonomic group. But any taxonomic group, even at the species level, can span several biovolume classes. Consequently, the use of a unique average biovolume misestimates the abundance and biomass of certain biovolume classes. The presence of these artefacts in size spectra based on average biovolumes is common in the literature (e.g. Marañón *et al.*, 2007; Huete-Ortega *et al.*, 2010). We suggest that these artefacts can be avoided by considering the distribution of cell biovolume within each taxon. We have shown that even if we lack the actual biovolume distribution, making gross approximations of the distribution of biovolumes removes these artefacts from the size spectra. Taxonomists usually have some knowledge about biovolume distributions, since they have measured a representative number of cells, sometimes even for several size classes within each taxonomic group (Olenina *et al.*, 2006). Our advice is not to lose this information by summarizing it in an average value, but to use it to obtain more realistic size spectra. The use of average cell biovolumes to assign a biovolume value to each of the cells counted does not significantly affect the estimated slope of the size spectrum, but it can affect the biological and/or ecological parameters derived from the intercept of the size spectrum, such as the standing stock of phytoplankton. It also introduces significant differences in the estimates of abundance and biomass of specific biovolume classes and can generate deviations from the linearity of the phytoplankton size structure.

Another problem with microscopy-based methods for characterizing size structure is the need for sample preservation. Changes in cell size and shape in response to the use of fixatives have been reported extensively (Leakey *et al.*, 1994; Montagnes *et al.*, 1994; Stoecker *et al.*, 1994; Menden-Deuer *et al.*, 2001) and also in samples analysed with FlowCAM (Zarauz and Irigoien, 2008). The absence of differences in the size spectra obtained from preserved samples with FlowCAM and microscopy suggests that both methodologies are closely comparable when applied to samples with the same preservation and classified by an expert. Hence, the effect of fixatives can explain the differences between fresh samples analysed with FlowCAM and preserved samples analysed with microscopy. The inaccuracy in the automatic classification of FlowCAM images is another source of error, which is likely to be reduced as image classification algorithms improve. Additionally, the representativeness of the sampled volume needs further study to develop protocols that are more robust in order to avoid undersampling. Although with the data presented in this work these sources of error are indistinguishable, the degree to which they affect the results provided by each of the FlowCAM working modes permits us to outline their relative importance.

Samples analysed with FlowCAM in autoimage mode are illustrative of the discrepancies between microscopy and FlowCAM. At the lower size limit of the nanoplankton fraction, the effect of fixatives on the inverted microscope samples causes an underestimation of cell numbers, resulting in flatter spectra than those obtained with FlowCAM. On the other hand, the images digitized in autoimage mode are classified with less accuracy than under the microscope, and many non-living particles are classified as living cells. This error is especially problematic in the smaller biovolume classes for which image quality is less and translates as steeper spectra. In addition, in the FlowCAM data, the sampled volume is insufficient to cover the whole spectrum, and the upper limits of the nanoplankton and the microplankton size ranges suffer from undersampling. In microscopy, the sedimentation method and the possibility of changing magnification during the sample analysis allow good estimation of particle abundances across the complete size range. Hence, since traditional microscopy underestimates the cell abundance and biomass (due to preservation) and the FlowCAM overestimates the cell abundance and biomass (due to classification of non-living particles), the actual slopes of size spectra lie between those from the two methods. The overall slope of the NASS reported by Blanco *et al.* (Blanco *et al.*, 1994) in a size spectrum including size distribution information from samples with multiple origins was -1.98. That value is intermediate between our -1.77 for preserved samples analysed with microscopy and our -2.11 for fresh samples analysed in autoimage mode.

The fluorescence-triggered FlowCAM mode provides a better estimation of cell abundance in the smaller biovolume classes than the autoimage mode. The presence of red fluorescence in planktonic cells is an unambiguous discriminatory variable to distinguish living autotrophic particles, avoiding the effects in autoimage mode of reduced optical resolution and the contamination by detritus. The larger sampled volume permits good coverage of the complete size range, with fewer missing biovolume classes than in the autoimage mode. As expected, the overall slope of the NASS in our data from the fluorescence-triggered mode, -1.99, is closer to the value of -1.98 reported by Blanco *et al.* (Blanco *et al.*, 1994). The effects of uncertainties in cell enumeration should be minimal when an ample size range of planktonic organisms (from pico- to macroplankton) is included in the analysis and several methodologies enumerate them. The global trend that arises compensates for the method-specific biases in nano- and microplankton estimation. However, in marine ecosystems, most size spectrum studies have been conducted at local scales and/or for only a small size range of planktonic organisms. In those cases, biases affecting the enumeration of the target size range can determine the estimated values of sample parameters.

The diversity indexes presented add a new facet to the capacities of automatic classification. The *a priori* selection of classification groups and the lower taxonomic resolution provided by automatic image classification derived from FlowCAM caution against its use in biodiversity studies. Despite these limitations, we have shown that estimates of taxonomic richness derived from FlowCAM are reasonably comparable with those obtained by microscopy. This opens the possibility to use a simple index obtained with FlowCAM to determine the variations of community diversity at large scales where sampling using traditional microscopy is not feasible. Some authors have used indices of taxonomic richness (e.g. mean number of species) as an indicator of community diversity and changes in ecosystem function (Beaugrand *et al.*, 2000), even though they do not reflect the actual number of taxa. For higher-order indices, such as the Shannon index, which include in their calculation both the number of taxa and their relative abundances, the difference between the two methods is larger, because the uncertainties in cell enumeration explained above affect the abundance values.

Scope of application of FlowCAM

Relevant information has been gathered in recent years about the comparability of FlowCAM and traditional methods. Nevertheless, when designing a sampling strategy, deciding whether FlowCAM is a reliable option remains challenging. We have reviewed the aspects in which it differs from microscopy in order to provide a global vision of the abilities of the automated technique and to help establish in which situations FlowCAM can substitute and/or complement microscopy with reliability and in which not.

FlowCAM has been used with success in several research scenarios. Its counting accuracy has been proved for cultures (Buskey and Hyatt, 2006) and natural samples (See *et al.*, 2005; Ide *et al.*, 2008). And it has given comparable results in cell sizing when compared with light microscopy (Sieracki *et al.*, 1998; Spaulding *et al.*, 2012). Hence, FlowCAM has become a useful tool in size-related studies needing extensive numeric information from the samples (Chisholm, 1992), particularly size structure determination (Álvarez *et al.*, 2011). In the current work, we have shown how routine application of FlowCAM analysis can provide results comparable with those obtained with light microscopy, not only in size structure determination but also in the discrimination of broad categories within the nano- and microplankton community, such as functional classes or autotrophic cells. However, although the overall error in the automatic classification of FlowCAM images is around 10% (Blaschko *et al.*, 2005; Zarauz *et al.*, 2009; Álvarez *et al.*, 2012), the number of categories that FlowCAM discriminates is still very low when compared with light microscopy. This limits its application in research scenarios that demand extensive taxonomic detail.

When used in studies for which their limits are acceptable, the results obtained with the two methods are comparable with each other, supporting the confident application of FlowCAM methodology. Although the fully automatic method seems appropriate for the analysis of variations in the planktonic community at broad spatial and temporal scales, further work is needed to standardize the protocols to avoid undersampling and to improve the automated classification of particles. The currently applied protocols are a weak point when dealing with waters with very low concentrations of particles. Such oligotrophic environments need substantial sample concentration to be properly characterized by FlowCAM. The reliable use of the FlowCAM for very dilute samples needs further protocol development.

CONCLUSIONS

FlowCAM is a useful advance for size structure studies, providing a way to analyse many samples in a reasonable amount of time and to obtain extensive numeric information. It is also capable of differentiating broad

taxonomic categories. However, the automatic classification of FlowCAM images currently only attains a low taxonomic resolution, thus when the aim is high taxonomic resolution, microscopy is still the unique choice. When limited to scenarios for which the two methodologies are comparable, ancillary factors must be considered to choose the most suitable technique: the scale of variation of the target variables, the time available for analysis, the possibility of analyzing fresh samples, the dependence on the operator and the need to discriminate the autotrophic community. The scope of application of the FlowCAM cannot be elucidated completely with the available literature, since that depends on methodological considerations needing further study. However, FlowCAM complements traditional techniques by improving the sampling resolution available for study of highly dynamic communities and providing the detailed descriptions of particle-size spectra necessary for ecological studies.

SUPPLEMENTARY DATA

Supplementary data can be found online at http://plankt.oxfordjournals.org.

REFERENCES

Álvarez, E., López-Urrutia, A., Nogueira, E. *et al.* (2011) How to effectively sample the plankton size spectrum? A case study using FlowCAM. *J. Plankton Res.*, **33**, 1119–1133.

Álvarez, E., López-Urrutia, A. and Nogueira, E. (2012) Improvement of plankton biovolume estimates derived from image-based automatic sampling devices: application to FlowCAM. *J. Plankton Res.*, **34**, 454–469.

Beaugrand, G., Reid, P. C., Ibañez, F. *et al.* (2000) Biodiversity of North Atlantic and North Sea calanoid copepods. *Mar. Ecol. Prog. Ser.*, **204**, 299–303.

Benfield, M. C., Grosjean, P., Culverhouse, P. *et al.* (2007) RAPID: research on automated plankton identification. *Oceanography*, **20**, 12–26.

Bérard-Therriault, L., Poulin, M. and Bossé, L. (1999) *Guide d'identification du phytoplancton marin de l'estuaire et du Golfe du Saint-Laurent*. CNRC-NRC, Otawa, Canada, pp. 387.

Blanco, J. M., Echevarría, F. and García, C. M. (1994) Dealing with size-spectra: some conceptual and mathematical problems. *Sci. Mar.*, **58**, 17–29.

Blaschko, M. B., Holness, G., Mattar, M. A. *et al.* (2005) Automatic in situ identification of plankton. *Proceedings of the Seventh IEEE Workshops on Application of Computer Vision (WACV/MOTION'05)*, **1**, 79–86.

Buskey, E. J. and Hyatt, C. J. (2006) Use of the FlowCAM for semi-automated recognition and enumeration of red tide cells (*Karenia brevis*) in natural plankton samples. *Harmful Algae*, **5**, 685–692.

Cermeño, P. and Figueiras, F. G. (2008) Species richness and cell-size distribution: size structure of phytoplankton communities. *Mar. Ecol. Prog. Ser.*, **357**, 79–85.

Chisholm, S. W. (1992) Phytoplankton size. In Falkowski, P. G. and Woodhead, A. D. (eds), *Primary Productivity and Biogeochemical Cycles in the Sea*. Plenum Press, New York, pp. 213–237.

Culverhouse, P. F. R. W., Reguera, B., Herry, V. *et al.* (2003) Do experts make mistakes? A comparison of human and machine identification of dinoflagellates. *Mar. Ecol. Prog. Ser.*, **247**, 17–25.

Cupp, E. E. (ed) (1977) *Marine Plankton Diatoms of the West Coast of North America*. Otto Koeltz Science Publishers, Koenigstein, Germany, pp. 237.

Dodge, J. D. (ed) (1982) *Marine Dinoflagellates of the British Isles*. Her Majesty's Stationary Office, London, United Kingdom, pp. 303.

Dodson, A. N. and Thomas, W. H. (1978) Reverse filtration. In Sournia, A. (ed.), *Phytoplankton Manual*. UNESCO, Paris, pp. 104–107.

Edler, L. and Elbrächter, M. (2010) The Utermöhl method for quantitative phytoplankton analysis. In Karlson, B., Cusack, C. and Bresnan, E. (eds), *Microscopic and Molecular Methods for Quantitative Phytoplankton Analysis*. UNESCO, Paris, pp. 13–20.

García, C. M., Jimenez-Gómez, F. and Rodríguez, J. (1994) The size-structure and functional composition of ultraplankton and nanoplankton at a frontal station in the Alboran Sea. Working groups 2 and 3 report. *Sci. Mar.*, **58**, 43–52.

Hillebrand, H., Dürselen, C.-D., Kirschtel, D. *et al.* (1999) Biovolume calculation for pelagic and benthic microalgae. *J. Phycol.*, **35**, 403–4424.

Huete-Ortega, M., Marañon, E., Varela, M. *et al.* (2010) General patterns in the size scaling of phytoplankton abundance in coastal waters during a 10-year time series. *J. Plankton Res.*, **32**, 1–14.

Ide, K., Takahashi, K., Kuwata, A. *et al.* (2008) A rapid analysis of copepod feeding using FlowCAM. *J. Plankton Res.*, **30**, 275–281.

Jakobsen, H. H. and Carstensen, J. (2011) FlowCAM: sizing cells and understanding the impact of size distributions on biovolume of planktonic community structure. *Aquat. Microb. Ecol.*, **65**, 75–87.

Leakey, R. J. G., Burkill, P. H. and Sleigh, M. A. (1994) A comparison of fixatives for the estimation of abundance and biovolume of marine planktonic ciliate populations. *J. Plankton Res.*, **10**, 375–389.

Legendre, P. and Legendre, L. (1998) *Numerical Ecology.* Elsevier Science B. V., Amsterdam.

Marañón, E., Cermeño, P., Rodríguez, J. *et al.* (2007) Scaling of phytoplankton photosynthesis and cell size in the ocean. *Limnol. Oceanogr.*, **52**, 2190–2198.

Menden-Deuer, S., Lessard, E. J. and Satterberg, J. (2000) Carbon to volume relationships for dinoflagellates, diatoms and other protist plankton. *Limnol. Oceanogr.*, **45**, 569–579.

Menden-Deuer, S., Lessard, E. J. and Satterberg, J. (2001) Effect of preservation on dinoflagellate and diatom cell volume and consequences for carbon biomass predictions. *Mar. Ecol. Prog. Ser.*, **222**, 41–50.

Moberg, E. A. and Sosik, H. M. (2012) Distance maps to estimate cell volume from two-dimensional plankton images. *Limnol. Oceanogr. Meth.*, **10**, 278–288.

Montagnes, D. J. S., Berges, J. A., Harrison, P. J. *et al.* (1994) Estimating carbon, nitrogen, protein and chlorophyll a from volume in marine phytoplankton. *Limnol. Oceanogr.*, **39**, 1044–1060.

Olenina, I., Hajdu, S., Edler, L. *et al.* (2006) Biovolumes and size-classes of phytoplankton in the Baltic Sea. *HELCOM Balt. Sea Environ. Proc.*, **106**, 144.

See, J. H., Campbell, L., Richardson, T. L. *et al.* (2005) Combining new technologies for determination of phytoplankton community structure in the northern Gulf of Mexico. *J. Phycol.*, **41**, 305–310.

Sieracki, C. K., Sieracki, M. E. and Yentsch, C. S. (1998) An imaging-in-flow system for automated analysis of marine microplankton. *Mar. Ecol. Prog. Ser.*, **168**, 285–296.

Spaulding, S. A., Jewson, D. H., Bixby, R. J. *et al.* (2012) Automated measurement of diatom size. *Limnol. Oceanogr. Meth*, **10**, 882–890.

Stoecker, D. K., Gifford, D. J. and Putt, M. (1994) Preservation of marine planktonic ciliates: losses and cell shrinkage during fixation. *Mar. Ecol. Prog. Ser.*, **110**, 293–299.

Sun, J. and Liu, D. (2003) Geometric models for calculating cell biovolume and surface area for phytoplankton. *J. Plankton Res.*, **25**, 1331–1346.

Tomas, C. R. (ed) (1997) *Identifying Marine Phytoplankton.* Academic Press, San Diego, CA, pp. 858.

Utermöhl, H. (1958) Zur Vervollkommnung der quantitativen Phytoplankton-Methodik. *Mitt. Int. Ver. Theor. Angew. Limnol.*, **9**, 1–38.

Vuorio, K., Lepisto, L. and Holopainen, A.-L. (2007) Intercalibrations of freshwater phytoplankton analyses. *Boreal Environ. Res.*, **12**, 561–569.

Willén, E. (1976) A simplified method of phytoplankton counting. *Br. Phycol. J.*, **11**, 265–278.

Zarauz, L. and Irigoien, X. (2008) Effects of lugol's fixation on the size structure of natural nano–microplankton samples, analyzed by means of an automatic counting method. *J. Plankton Res.*, **30**, 1297–1303.

Zarauz, L., Irigoien, X. and Fernandes, J. A. (2009) Changes in plankton size structure and composition, during the generation of a phytoplankton bloom, in the central Cantabrian sea. *J. Plankton Res.*, **31**, 193–207.